High–Q^2 and High–P_T Processes at HERA

Martin zur Nedden[1]
Deutsches Elektronen Synchrotron DESY, Hamburg Germany
on behalf of the H1 and ZEUS Collaborations

Deep inelastic $e^{\pm}p$ scattering at high squared momentum transfer Q^2 at the electron–proton collider HERA at DESY is used to test aspects of the Standard Model with about 100 pb^{-1} of data available to each of the collider experiments H1 and ZEUS. The inclusive single and double differential cross sections for neutral and charged current processes are measured and the structure function $x\tilde{F}_3$ is extracted. The data are found to be in good agreement with the Standard Model predictions. The measurements at very high Q^2 ($>$ 5000 GeV^2) are used to search for $eeqq$ contact interactions with scales not directly accessible at HERA. A search for gravitational effects mediated through the exchange of virtual gravitons which propagate into large extra dimensions is presented. Finally, a search for direct production of scalar and vector leptoquark, coupling to first generation fermions, is performed in the region of very high Q^2. Investigations of direct W boson production in the process $ep \to eWX$ are performed. Anomalous single top production mediated by a flavor changing neutral current is also searched for.

[1]E-mail address: nedden@mail.desy.de

1 Introduction

The electron–hadron collider HERA extends the study of inclusive deep inelastic (DIS) neutral (charged) current interaction $ep \to e(\nu)X$ up to very high squared momentum transfers Q^2. The DIS cross sections are sensitive to the proton structure and QCD dynamics. In the past 6 years HERA has been running with beams of both lepton charges ($e^{\pm}$) and with two different center of mass energies ($\sqrt{s}$ = 300/320 GeV) by increasing the proton beam energy from 820 GeV to 920 GeV. The collider experiments H1 and ZEUS have made use of the luminosity (about 100 pb^{-1} per experiment) to extend the phase space into unexplored kinematic regions of high Q^2 and small x, where x is the Bjorken scaling variable. The large integrated luminosity collected enables the experiments to extend the measurements to the highest Q^2 where distances of proton structure at the order of 10^{-18} m are probed. At large Q^2 new phenomena not directly accessible may become observable as deviations from the Standard Model (SM) predictions. In addition, in the region where $Q^2 \simeq M^2_{Z,W}$, the Z^0 and $W^{\pm}$ masses squared, effects of the electroweak sector of the SM can be tested.

1.1 Kinematics

The kinematics of DIS processes can be described using the squared momentum transfer Q^2, the Bjorken scale variable x of the struck quark in the quark parton–model (QPM), the inelasticty y and the squared center of mass energy s:

$$Q^2 = -q^2 = (k - k') \qquad x = \frac{Q^2}{2p \cdot q} \qquad y = \frac{p \cdot q}{p \cdot k} \qquad s = (p + k)^2 \quad (1)$$

with $k(k')$ and p being the four momentum of the incident (scattered) lepton and proton. These variables are related via:

$$Q^2 = s \cdot x \cdot y \quad (2)$$

In Fig. 1 the kinematic plane of HERA is shown, demonstrating the accessible phase space in x and Q^2 and the overlap with a number of fixed–target experiments. In the

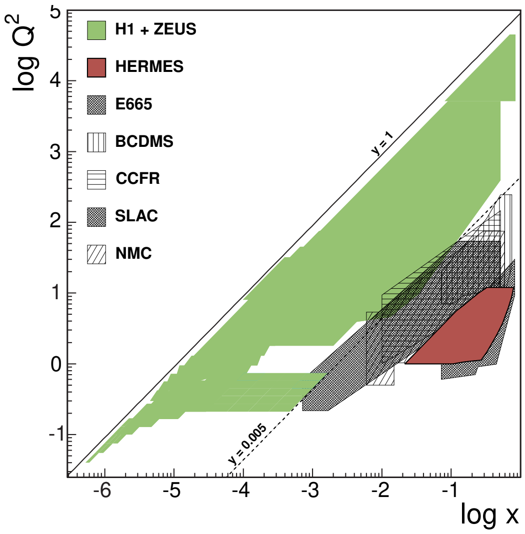

Fig. 1: *The kinematic region of HERA and the overlap to the earlier fixed–target experiments*

high Q^2 region searches for new phenomena beyond the SM can be done, as well as probing physics in the region where the electromagnetic (γ bosons) and the weak ($W^{\pm}$, Z^0 bosons) interactions are of comparable strength.

2 High Q^2 Processes

2.1 Cross Sections

The neutral current (NC) Born cross section [1] for the processes $e^{\pm}p \to e^{\pm}X$ with unpolarized beams is given by [2, 3]

$$\frac{d^2\sigma_{NC}(e^{\pm})}{dxdQ^2} = \frac{2\pi\alpha^2}{xQ^4}(Y_+\tilde{F}_2^{NC} \mp Y_- x\tilde{F}_3^{NC} - y^2\tilde{F}_L^{NC}) \cdot (1+\delta_{NC}^{weak}) \tag{3}$$

where α is the fine structure constant, $Y_{\pm} \equiv 1 \pm (1-y)^2$ contains the helicity dependence of the electroweak interaction and δ_{NC}^{weak} are the weak radiative corrections described in [4]. The generalized structure functions $\tilde{F}_2$ and $x\tilde{F}_3$ consist of contributions of the γ and Z interactions and the γ/Z interference term [6]:

$$\tilde{F}_2 \equiv F_2 - v_e \frac{\kappa_w Q^2}{(Q^2+M_Z^2)} F_2^{\gamma Z} + (v_e^2 + a_e^2)(\frac{\kappa_w Q^2}{Q^2+M_Z^2})^2 F_2^Z \tag{4}$$

$$x\tilde{F}_3 \equiv -a_e \frac{\kappa_w Q^2}{(Q^2+M_Z^2)} xF_3^{\gamma Z} + (2v_e a_e)(\frac{\kappa_w Q^2}{Q^2+M_Z^2})^2 xF_3^Z \tag{5}$$

Here v_e and a_e are the vector and axial couplings of the electron to the Z^0. The term κ_w is given by $\kappa_w^{-1} = 4\frac{M_W^2}{M_Z^2}(1-\frac{M_W^2}{M_Z^2})$ in the on–shell scheme [5]. The dominant contribution to the cross section in the kinematic domain at HERA comes from the electromagnetic structure function F_2 originating from the γ exchange only. The contributions corresponding to Z^0 exchange are F_2^Z and xF_3^Z and the γZ^0 interference is given by $F_2^{\gamma Z}$ and $xF_3^{\gamma Z}$. The contribution of the longitudinal structure function $\tilde{F}_L$ [7] is significant at high y and is expected to diminish in the high Q^2 region. The structure function $x\tilde{F}_3$ contributes only in the high Q^2 region of Z^0 exchange.

In the QPM the structure functions F_2 are related to the sums of the quark and anti–quark densities:

$$[F_2, F_2^{\gamma Z}, F_2^Z] = x\sum_q [e_q^2, 2e_q v_q, v_q^2 + a_q^2](q+\bar{q}) \tag{6}$$

and the structure functions xF_3 to the difference between quark and anti–quark densities:

$$[xF_3^{\gamma Z}, xF_3^Z] = x\sum_q [2e_q a_q, 2v_q a_q](q-\bar{q}), \tag{7}$$

where q and $\bar{q}$ are the parton distributions functions (PDFs) for quarks and anti–quarks, e_q is the charge of quark q in units of the electron charge and v_q and a_q are the vector and axial–vector couplings of the quark. $x\tilde{F}_3$ is thus sensitive to the "pure" valence quark content $(q-\bar{q})$ in the proton, and its contribution is sensitive to the lepton charge (Eq. 3), while $\tilde{F}_2$ is the same for electron and positron scattering.

The double differential charged current (CC) cross section for the reactions $e^{\pm}p \to \nu X$ is suppressed compared to the NC cross section in the low Q^2 region due to the high $W^{\pm}$ mass entering in the propagator [2, 8]:

$$\frac{d^2\sigma_{CC}(e^{\pm})}{dxdQ^2} = \frac{G_F^2}{2\pi x}(\frac{M_W^2}{Q^2+M_W^2})^2 \times \Phi_{CC}^{\pm}(x,Q^2)(1+\delta_{CC}^{weak}) \tag{8}$$

where the CC structure function term $\Phi_{CC}^{\pm}$ is given by:

$$\Phi_{CC}^{\pm}(x,Q^2) = \frac{1}{2}(Y_+\tilde{W}_2^{\pm} \mp Y_- x\tilde{W}_3^{\pm} - y^2\tilde{W}_L^{\pm}). \tag{9}$$

Here G_F is the Fermi coupling constant and δ_{CC}^{week} are the weak radiative corrections. The structure functions for CC interactions $\tilde{W}_2$, $x\tilde{W}_3$ and $\tilde{W}_L$ are defined in analogy to the NC case. Neglecting the contribution of heavier quarks (t and b quarks) Φ_{CC} can be written as:

$$\Phi_{CC}^{+} = x\cdot[(\bar{u}+\bar{c})+(1-y)^2(d+s)], \qquad \Phi_{CC}^{-} = x\cdot[(u+c)+(1-y)^2(\bar{d}+\bar{s})] \tag{10}$$

where u, d, c and s are the quark and $\bar{u}$, $\bar{d}$, $\bar{c}$ and $\bar{s}$ are the anti–quark PDFs. As shown in Eq. 10, the CC cross section is sensitive to the lepton charge. At high x, the structure function term depends predominantly on the valence quark distribution. In the e^+ case, the d quark is probed, but suppressed by the factor $(1-y)^2$, whereas in the e^- case the u quark contribution is not suppressed.

It is convenient to remove the dominant Q^2 dependence of the boson propagator from the cross section to get the "reduced cross section":

$$\tilde{\sigma}_{NC}(x,Q^2) = \frac{xQ^4}{2\pi\alpha^2}\frac{1}{Y_+}\cdot\frac{d^2\sigma_{NC}}{dxdQ^2}, \quad \tilde{\sigma}_{CC}(x,Q^2) = \frac{2\pi x}{G_F^2}(\frac{M_W^2+Q^2}{M_W^2})^2\cdot\frac{d^2\sigma^{CC}}{dxdQ^2} \tag{11}$$

2.2 Neutral and Charged Current Measurements

The NC and CC cross sections $d\sigma/dQ^2$ are presented in Fig. 2 [2, 1, 3, 8, 9, 10, 11] covering a Q^2 range of more than two orders of magnitude. The data for e^+p and e^-p scattering are found to be in good agreement with the SM prediction. The e^+p data from the years $1994-1997$ were taken at $\sqrt{s}=300$ GeV. Since the proton beam energy was increased in 1998 from 820 GeV to 920 GeV the center of mass energy $\sqrt{s}$ for the $e^{\pm}p$ data of 1998 - 2000 is $\sqrt{s}=320$ GeV. For all cross sections, the effect of the increased p–beam energy is small. For comparison the data taken at $\sqrt{s}=300$ GeV were corrected to $\sqrt{s}=320$ GeV.

The difference between the e^-p and e^+p NC cross sections in Fig. 2 at high Q^2 is due to the Z^0 exchange leading to an enhancement of the e^-p cross section arising from the $x\tilde{F}_3$ term. In contrast, at lower Q^2 and x, the most important contribution arises from the sea quarks. The contributions of the sea quarks are flavor symmetric, hence the e^+p and e^-p NC cross sections are comparable. Also the CC cross sections in Fig. 2 are found to be higher for the e^-p case: at high Q^2 (high x) the contribution of valence quarks is dominant. As visible in Eq. 10, the $(1-y)^2$ factor for e^+–d quark scattering reduces the CC cross section in comparison to the unsuppressed and large u quark density in the e^- case.

For large Q^2 ($Q^2 > 5000$ GeV^2), where the $W^{\pm}$ and Z^0 squared masses are of the order of the squared momentum transfer, the NC and CC cross sections are of comparable strength as presented in the lower–most plot of Fig. 2.

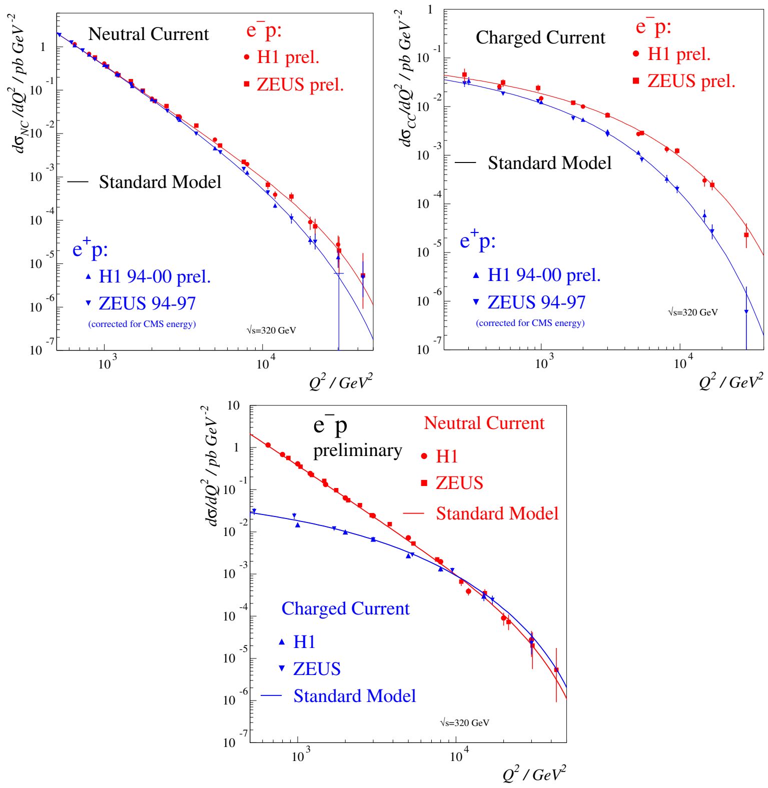

Fig. 2: *The Q^2 dependence of the NC and CC cross sections for $e^{\pm}p$ data, compared to the SM expectation. At high Q^2, NC and CC cross sections are comparable (electroweak unification).*

The differential NC and CC cross section as a function of x are shown in Fig. 3 for both e^+p and e^-p scattering [1, 9, 10, 11]. The NC data are shown for two different Q^2 cuts to demonstrate the electroweak part of the interaction in contrast to the pure γ exchange. For $Q^2 > 10000$ GeV^2 the γ/Z^0 interference contribution enhances the cross section in the e^-p case compared to the e^+p case as expected from Eq. 5. The difference of the CC cross sections reflects the different contributions of quark flavors probed by the exchanged $W^{\pm}$ bosons and the helicity structure of CC interactions (see Eq. 10).

The difference between the NC e^+p and e^-p cross sections at high Q^2 is displayed in Fig. 4 for different x values. At the same center of mass energy $\sqrt{s}$ the difference of the NC cross sections determines $x\tilde{F}_3$ directly. Due to the different proton beam energies

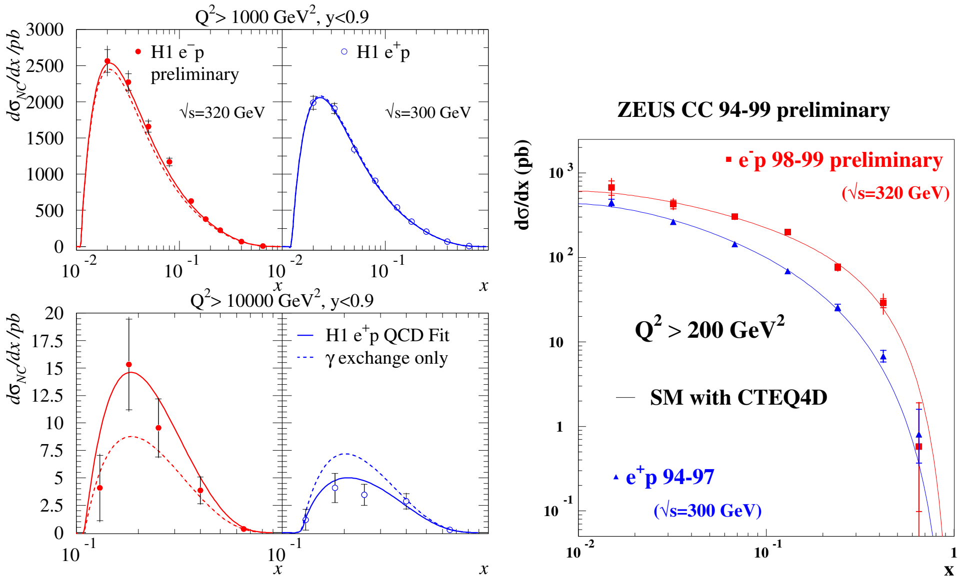

Fig. 3: *The single differential cross section $d\sigma/dx$ for both lepton polarities at two Q^2 values for NC (left, H1) and for CC (right, ZEUS). The solid curves show for the NC cross sections the SM expectation and the dashed curves the contribution of the photon exchange only.*

the structure function $x\tilde{F}_3$ was extracted using a small correction for fixed x and Q^2:

$$\tilde{\sigma}^-_{NC} - \tilde{\sigma}^+_{NC} = x\tilde{F}_3[\frac{Y_-^{920}}{Y_+^{920}} + \frac{Y_-^{820}}{Y_+^{820}}] - \tilde{F}_L[\frac{y^2_{920}}{Y_+^{920}} - \frac{y^2_{820}}{Y_+^{820}}] \qquad (12)$$

The contribution of $\tilde{F}_L$ is found in QCD calculations to be below 1% over most of the kinematic region considered in this analysis. The resulting structure function $x\tilde{F}_3$ increases with Q^2 at fixed x due to the Z^0 propagator.

Measurements of $x\tilde{F}_3$ at high Q^2 in different x bins are shown in Fig. 5 [1, 10] using Eq. 12. In order to reduce statistical fluctuation, the number of bins was reduced compared to the measurement of the double–differential cross sections. $x\tilde{F}_3$ is presented at fixed values of Q^2 as a function of x. As discussed above, the term of $\tilde{F}_L$ gives a correction to $x\tilde{F}_3$ due to the changed p–beam energies, but this is small and therefore negligible compared to the statistical uncertainty. As in Fig. 4 the data are well described by the SM predictions, evaluated using either the CTEQ4D or the MRST(99) parton momentum distributions.

The double differential charged current cross section $d^2\tilde{\sigma}_{CC}/dxdQ^2$ for the e^+p data is presented in Fig. 6 [9]. The corresponding ZEUS results can be found in [3]. As expected from charge conservation the cross section is dominated at high x by d quark scattering. The rise of $\tilde{\sigma}_{CC}$ with decreasing x can be explained by the contributions from the sea. At low x (high y) the d and s quark contributions are suppressed by the

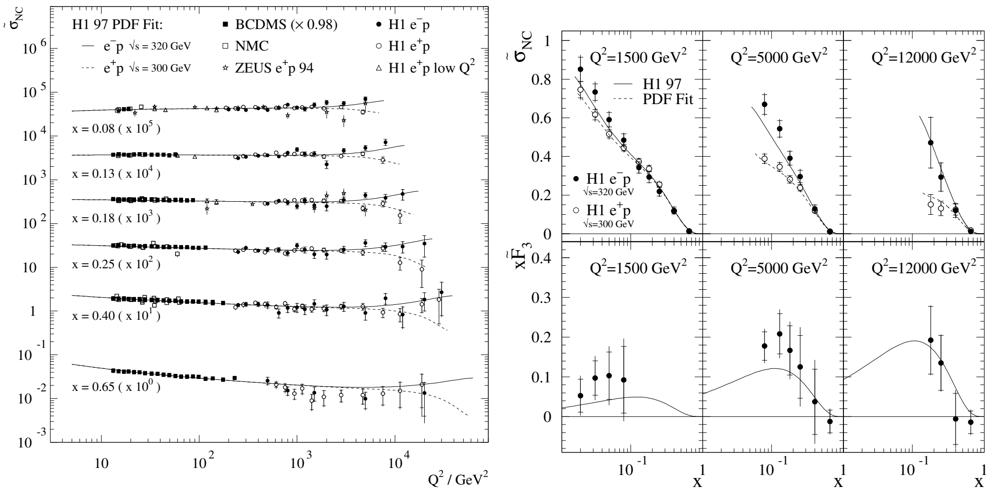

Fig. 4: *The NC reduced cross section $\tilde{\sigma}_{NC}(x, Q^2)$ at high x compared with the H1–PDF fit for three different Q^2–values. The structure function $x\tilde{F}_3$ is compared to the H1–97–PDF fit.*

factor $(1-y)^2$ (see Eq. 10).

Presently, the behavior of the d/u ratio in the valence quark region at high x is still not well–known. Using the recent HERA e^+p data the u and d quark distributions can be extracted using the NC and CC cross section at high Q^2 with minimal assumptions. The density of sea quarks is small at high x. At high x, the structure function Φ_{NC} is primarily sensitive to the u quark density since the d quark contribution is suppressed by the quark charge squared:

$$\tilde{\sigma}_{NC}(e^+) \quad \propto \quad \Phi_{NC} \propto (1 + (1-y)^2) \sum e_i^2 \cdot x \cdot q_i \qquad (13)$$

$$\tilde{\sigma}_{CC}(e^+) \quad \propto \quad \Phi_{CC} \propto x \cdot \bar{u} + (1-y)^2 \cdot x \cdot d \qquad (14)$$

On the other hand, the structure function Φ_{CC} is sensitive mainly to the d quark density, since the u quark does not contribute in $e^+p \to \nu X$ scattering (see Eq. 10). In Fig. 7 [2, 9] the NC and CC structure functions and their dominant terms Φ_{NC}^u and Φ_{CC}^d, representing the contributions of u and d quark densities, respectively, and the predictions from a fit to the low Q^2 data are shown at $x = 0.25$ and $= 0.40$. The dominant quark densities $xu(x)$ and $xd(x)$ are extracted from the data by comparison to the predictions of the low–Q^2 fit using the $\overline{MS}$ scheme. The results in Fig. 7 provide an indication of the current sensitivity to the d–quark density at high x. A more precise measurement of the d quark density will be possible with the luminosity upgrade at HERA (see Ch. 5).

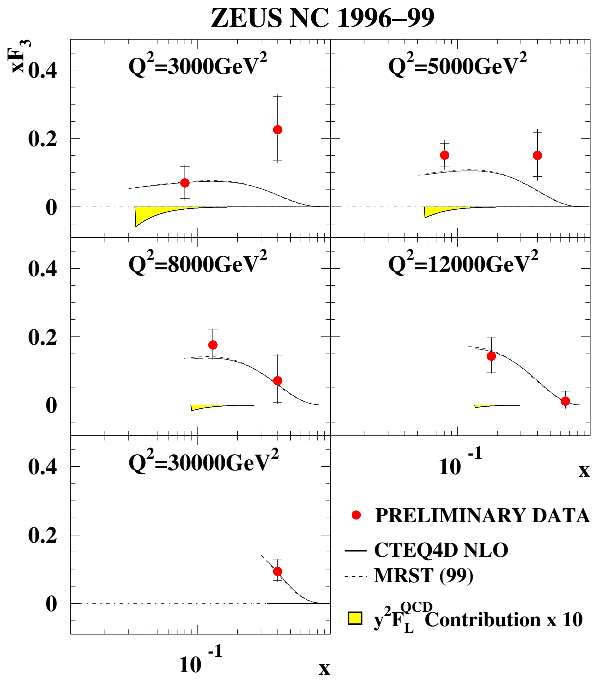

Fig. 5: *The structure function $x\tilde{F}_3$ compared to the SM prediction using CTEQ4D and MRST(99) parton distribution functions. The inner error bars represents the statistical errors, the outer the total errors. The contribution of $y^2 F_L$ calculated from QCD is shown in the shaded band increased by a factor of 10.*

3 Searches at very high Q^2

3.1 Contact Interactions

The well–measured NC cross section up to the highest accessible region of momentum transfer enables sensitive tests of the SM to be made. In the very high Q^2 region the structure of the eq interaction can be probed down to very short distances. At large scales new phenomena not directly accessible at HERA may become visible as deviations from the SM prediction. A well–known concept to assess the experimental sensitivity beyond the maximal available center of mass energy $\sqrt{s}$ and to parameterize indirect signatures of new physics phenomena beyond the SM is to parameterize the eventual new interaction as an effective 4–fermion contact interaction (CI) (see Fig. 8). Possible sources of a contact term are either the exchange of a new heavy particle or a substructure of the particles involved. The measured data are compared to the SM expectations and possible effects might be visible through interference with SM processes at even lower $\sqrt{s}$. The scale $\Lambda \gg \sqrt{s}$ can be related either to the mass and

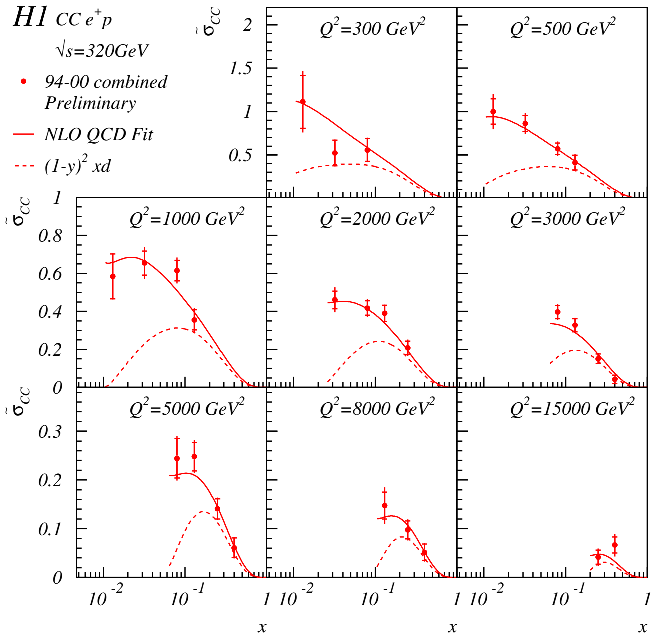

Fig. 6: *The reduced double differential CC cross section $\tilde{\sigma}_{CC}(x, Q^2)$ for the 94-00 combined data is shown and compared to the H1–NLO–QCD fit. The dashed line indicates the contribution of the valence quark.*

coupling of the exchanged massive new heavy particle or to the size of the substructure of the fermions involved in the interaction. In the search for CI phenomena particle density functions (PDF) are used which are measured at low Q^2 where the statistics is high and the theory is well–established (Chap. 2.2). The PDFs are extrapolated to high momentum transfers using QCD evolution, where deviations from the measured NC cross sections due to new phenomena could be most prominent.

The most general chiral invariant Lagrangian for NC vector–like CI can be written as [12]:

$$\mathcal{L}_{CI} = \sum_{i,j=L,R}^{q=u,d} \eta_{ij}^q (\bar{e}_i \gamma^\mu e_i)(\bar{q}_j \gamma_\mu q_j) \tag{15}$$

$$\Rightarrow \mathcal{L}_{tot} = \mathcal{L}_{SM} + \mathcal{L}_{CI} \tag{16}$$

with the effective coupling coefficients depending on a overall coupling strength g and a scale parameter $\Lambda_{i,j}^q$:

$$\eta_{ij}^q = \epsilon_{ij}^q \left(\frac{g}{\Lambda_{ij}^q}\right)^2 \tag{17}$$

where i, j denote the left/right–handed particles (chiralities) and the prefactor ϵ, com-

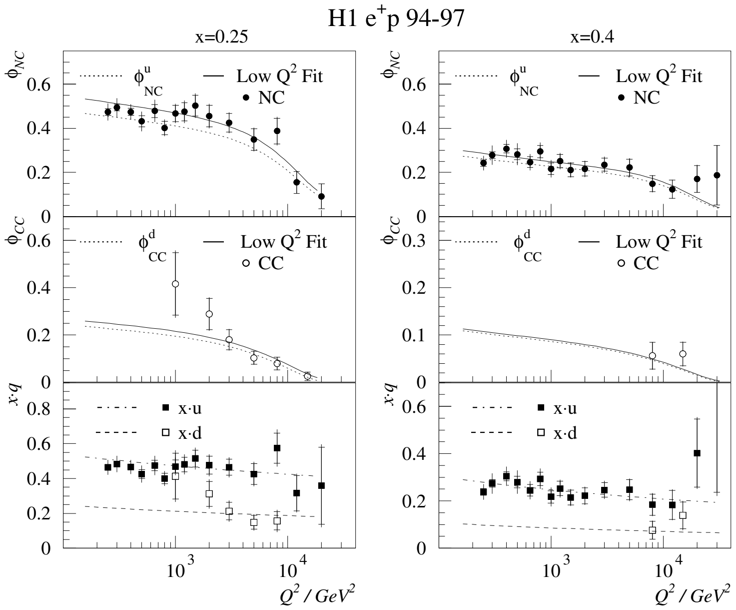

Fig. 7: *The structure functions Φ_{NC} and Φ_{CC} of the measured double differential cross sections are compared to the fit to the low Q^2 data. The extracted u and d quark densities are shown at two different x values.*

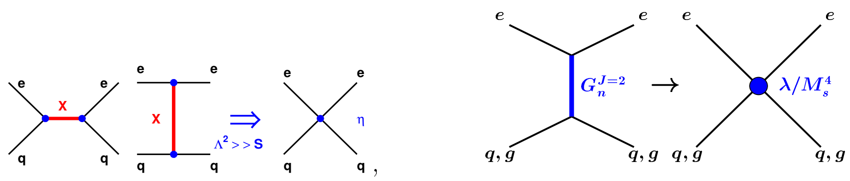

Fig. 8: *Feynman graphs for four–fermion (eeqq) contact interactions (left) and for the exchange of excited gravitons in models with large extra dimensions (right).*

monly set to $\epsilon = \pm 1$, determines the sign of the interference with the SM Lagrangian. The coupling strength g is set to $g^2 = 4\pi$ by convention. Only the first generation quark flavors $q = u, d$ are taken into consideration. Scalar and tensor couplings including helicity flip are already constrained beyond the energy scale of HERA and therefore not considered [12].

A possible fermion compositeness or substructure can be expressed through the η^q_{ij} parameters (see Eq. 17) which depend only on the ratio of the coupling constant g over the scales Λ^q_{ij}. The differential NC cross section $d\sigma/dQ^2$ is compared to the SM prediction and deviations are expressed in terms of model parameters [14, 15, 16, 19, 20, 21]. In order to derive quantitative tests a χ^2 analysis is performed taking the dominant error sources and uncertainties into account. According to Eq. 15 many combinations are possible. Besides pure chiral couplings the following vector and axial coupling combinations were considered:

- **VV**, **AA**, **VA**: vector / axial couplings
- $\boldsymbol{U_i}$: parity conserving combinations
- $\boldsymbol{X_i}$: same as $\boldsymbol{U_i}$ with $\boldsymbol{\eta_{ab}^{eu} = \eta_{ab}^{ed}}$

The summary of the upper limits are presented in Fig. 9 (left). Within two standard deviations the compositeness scale parameters ϵ/Λ^2 are compatible with the SM for all couplings investigated. The limits on the compositeness scales Λ^+ and Λ^- are also given in Fig. 9. They correspond to positive and negative interference with the SM and vary between 1.7 TeV and 5.0 TeV.

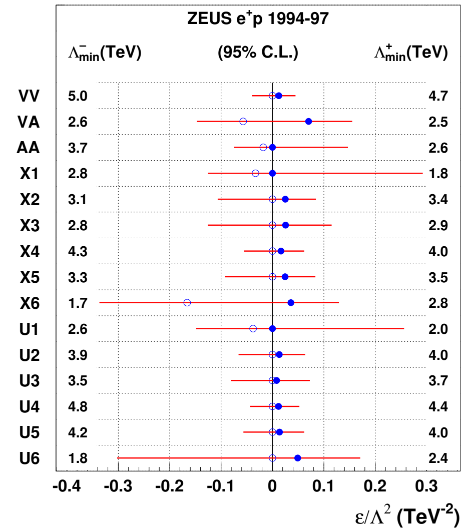

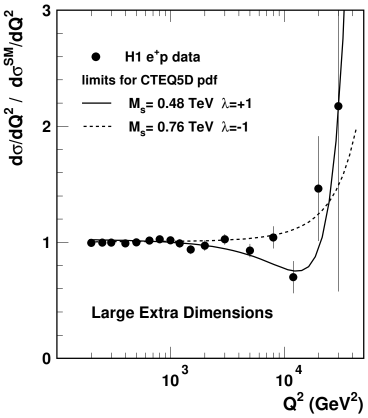

Fig. 9: *Results of the parameter ϵ/Λ^2 for various CI models (see text). On the right side, a fit to the NC cross section $d\sigma/dQ^2$ normalized to the SM expectation using the CTEQ5D parton density [18] is presented for the study of possible graviton exchange.*

3.2 Large Extra Dimensions

Another model of new phenomena is the exchange of gravitons coupling to SM particles, described as low scale quantum gravity effects propagating into extra spatial dimensions [13]. Gravity can be characterized by a scale $M_S \sim \mathcal{O}(\text{TeV})$ in $4+n$ dimensions for $n > 1$. The necessary extra spatial dimensions n are restricted to a volume of the size

R, and the scales in the 4 ordinary dimensions[1] and in the $4+n$ extra dimensions are related to the effective mass M_S by:

$$M_P^2 \sim R^n M_S^{2+n} \tag{18}$$

The reduction of the scale leads for $n>0$ to a modification of Newton's gravitational law at distances $r<R$, where the gravitational force would rise with $1/r^{2+n}$ and become measurable at the scale M_S. In the SM particles are confined to 4 dimensions. Only the massless graviton propagates as a spin–2 particle into the n additional dimensions. If the graviton is projected into the normal 4–dimensional space after compactification of the n extra dimensions, it appears as a spectrum of massive Kaluza–Klein states with masses $m^{(j)} = j/R$ which also include the zero–mass state. The effective CI coupling is the result of the summation over all Kaluza–Klein states j with masses up to the scale M_S compensating the huge $1/M_P$ suppression leading to an effective CI coupling of:

$$\eta_G \propto \frac{\lambda}{M_S^4} \tag{19}$$

The gravitational CI is very different from the conventional ones: the coupling constant η is, in contrast to Eq. 17, proportional to M^{-4} and the electron–gluon scattering is also included which is not present in the SM. The contribution of virtual gravition exchange to DIS has been derived from the cross sections given in [17]. In order to get the inclusive ep cross section all individual subprocesses, corresponding to pure graviton (G) exchange and γG– and ZG–interference, have to be integrated over the x depending parton distributions $q(x)$, $\bar{q}(x)$ and $g(x)$ (gluons). The expected gluon contribution to the gravitational effects is at the order of several percent at the highest Q^2.

The data analysis for the strength of virtual graviton exchange characterized by the ratio λ/M_S^4 is similar to the procedure described above by fitting the differential cross section with λ/M_S^4 as a free parameter. The lower limits on the effective mass scale are extracted at 95% CL by fitting $d\sigma/dQ^2$ with η_G (Eq. 19) as free parameter: $M_S > 0.48$ TeV for $\lambda = +1$ and $M_S > 0.72$ TeV for $\lambda = -1$. Here λ is set to $\pm$ 1 as the sign of the interference with SM particles is unknown. The sensitivity of the H1 data to large extra dimensions is presented in Fig. 9 (right).

3.3 Leptoquarks

Leptoquarks (LQ) are color triplet bosons of spin 0 or 1, carrying lepton (L) and baryon (B) number and fractional electric charge. A fermion number $F = L + 3B$ is defined, which takes the values of $F = 2$ for $e^- q$, $F = 0$ for $e^+ q$ and $e^- \bar{q}$ and $F = -2$ for $e^+ \bar{q}$ states. Generally, the LQ's are classified depending on their quantum numbers: $S^J_{L,R}/V^J_{L,R}$, where S/V stands for scalar/vector, J denotes the weak isospin of the LQ and L/R the chirality of the lepton coupled to the LQ.

At HERA, LQs can be produced resonantly in the s–channel or exchanged in the u–channel between incoming lepton and a quark coming from the proton. Both processes

[1] At the Planck mass $M_P \sim 10^{19}$ GeV gravitational interactions are comparable in strength to the other fundamental interactions.

interfere with the NC DIS cross sections. The resonant process presented here is valid as long as the LQ mass M_{LQ} is not too high and its width $\Gamma \propto \lambda_{LQ}^2 \cdot M_{LQ}$, where λ denotes the Yukawa coupling [26], is small enough. For $\sqrt{s} = 320$ GeV this is the case for M_{LQ} up to ≈ 290 GeV when the strength of λ is of the order of α_{em}.

In the s–channel, LQs are produced at the mass $M = \sqrt{s \cdot x}$. Scalar LQs decay isotropically in their rest frame leading to a flat $d\sigma/dy$ spectrum, where $y = Q^2/s \cdot x = \frac{1}{2}(1+\cos\vartheta^\star)$ and $\vartheta^\star$ is the decay polar angle of the lepton relative to the incident proton. On the other hand, the decay of vector LQs is distributed according to $d\sigma/dy \propto (1-y)^2$. The cross section of the dominant DIS NC photon exchange process at fixed x has the y dependence $d\sigma/dy \propto y^{-2}$ and is thus different from the scalar or vector LQ production.

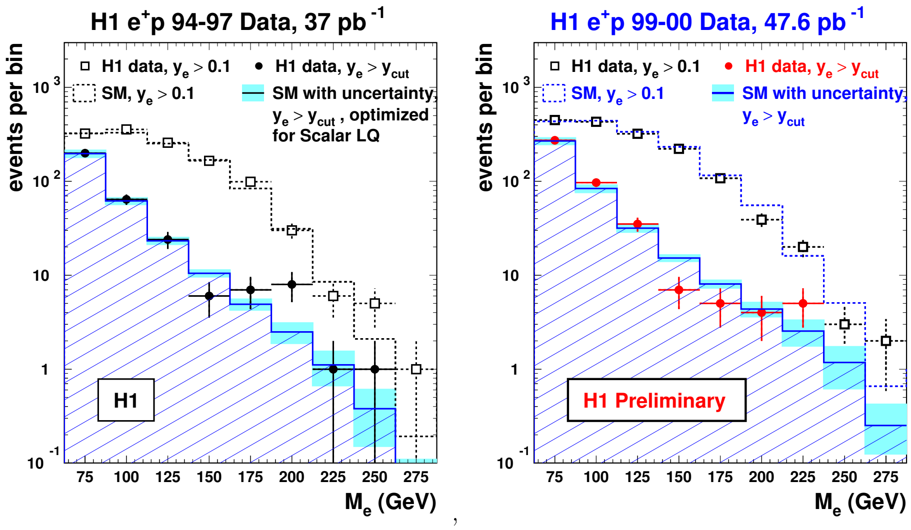

Fig. 10: *Mass spectra for NC DIS–like final states for data and SM expectation before and after a y cut (see text) was applied. The grey band indicates the $\pm 1\sigma$ error band.*

In Fig. 10 a comparison of the measured mass spectrum with the SM prediction is shown, before and after applying a mass dependent y_e cut[2] for the 94-97 and the 99-00 high Q^2 DIS data in the process $e^+p \to e^+ + X$. The cut $y_e > y_{cut}$ is designed to optimize the signal significance by finding the best compromise between an efficiency loss of the LQ signal and the background reduction. In the 94–97 e^+p data an excess of events was observed for masses around 200 GeV[26]. The excess was not confirmed by the new data (99–00)[22].

Since no evidence for direct production of LQ's is observed, the data are used to derive constraints on the Yukawa coupling at the lepton–quark–LQ vertex. Fig. 11 shows the H1 and ZEUS constraints on $\tilde{S}_{1/2,L}$ and $S_{0,L}$ LQ's following the Buchmüller–Rückl–Wyler [23] model and a comparison to constraints set at LEP and the TEVATRON [25].

[2] The subscript e is used here to indicate that the kinematics is reconstructed from the scattered positron.

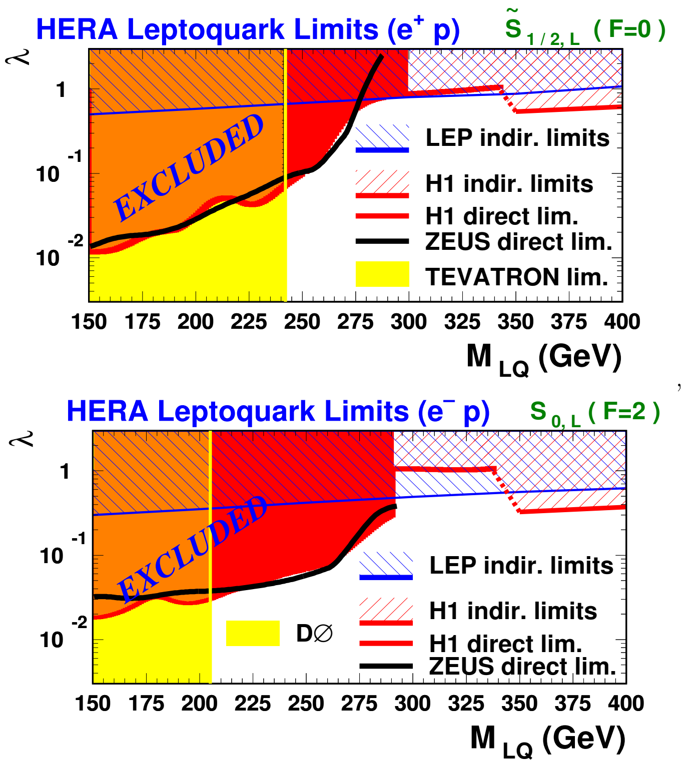

Fig. 11: *Mass–dependent exclusion limits at 95% CL on the Yukawa coupling* λ *for scalar LQ's from HERA, LEP and TEVATRON. The gray and hatched regions are excluded. In the notation* $S_{I,L/R}$ *I denotes the weak isospin* $I = 0, 1/2, 1$ *and* L/R *denotes the lepton chirality.*

At LEP, virtual LQ exchange has been studied in e^+e^- annihilation experiments [24]. Bounds derived by H1 via CI (see Chap. 3.1) complementing the direct searches of LQ's are also shown [26] for LQ masses above 350 GeV. The coupling limits are compatible with each other in the mass region where they overlap.

4 High P_T Leptons

Since the H1 and ZEUS experiments have collected a large amount of luminosity they are sensitive to rare SM processes such as direct W–production. Non standard processes leading to similar topologies have also been investigated.

4.1 W production

A search for W boson production in the process $ep \to eWX$ with subsequent W decay into electrons or muons has been reported in [27, 28] based on a integrated luminosity of 95 pb^{-1} and 82 pb^{-1} for H1 and ZEUS, respectively. The main characteristics of the W candidates are an isolated lepton and missing transverse momentum due to the ν, which escapes detection, originating from the W decay. The Feynman graph of the process is shown in Fig. 12 left. H1 observes an excess at large transverse momenta of the hadronic system P_T^X, where ZEUS finds agreement with the SM predictions. H1 has reported before such an excess based on a smaller event sample [29].

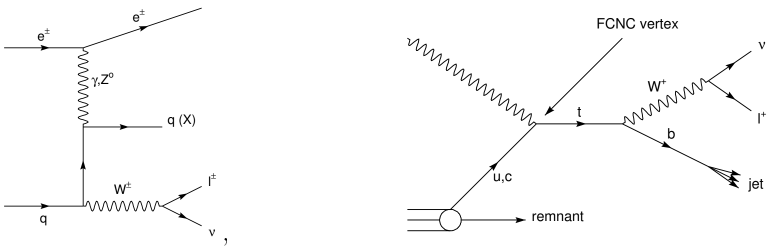

Fig. 12: *Feynman graphs of direct W (left) and single top production (right) via the flavor changing neutral current (FCNC).*

In Fig. 13 three distributions are presented for the selected events: the distribution of the transverse momentum of the system X, P_T^X, for the μ channel in case of ZEUS, for the e and μ channels in case of H1 and of the transverse mass M_T for the neutrino–lepton system for H1 only. The ZEUS P_T^X distribution is in good agreement with the SM expectation at small P_T^X, which is dominated by the two–photon process $ep \to e\mu^+\mu^-X$. The P_T^X distribution or the W candidates of H1 indicates clearly an excess of events in the region of high P_T^X. The events of H1 generally have a large measured M_T centered around the W mass. The shape of the M_T distribution is well described by the SM prediction.

In contrast to H1, ZEUS observes 11 W candidates in good agreement with the SM expectation of 9.8 events which include 2.7 expected W–events. Seven of these events are in the e–channel (SM: 6.1 ± 0.9) and four are in the μ–channel (SM: 3.7 ± 0.4). The measurement of H1 contains 14 events to be compared to a SM expectation of 8.2 including 6.4 W–events. The excess above the SM expectation originates from the high P_T^X region. Above $P_T^X > 25$ GeV, 9 events are measured by H1 to be compared to the SM expectation of 2.3 ± 0.6. To make the SM predictions comparable, H1 and ZEUS repeated their analyses with the same cuts. The excess in the high P_T^X region remains in the case of H1, whereas ZEUS is still in good agreement with the SM, although the SM expectations are the same for H1 and ZEUS for this analysis (see Tab. 1). This shows that the differences between H1 and ZEUS cannot be assigned to different phase space. More statistics is needed to reduce the uncertainty (see Ch. 5).

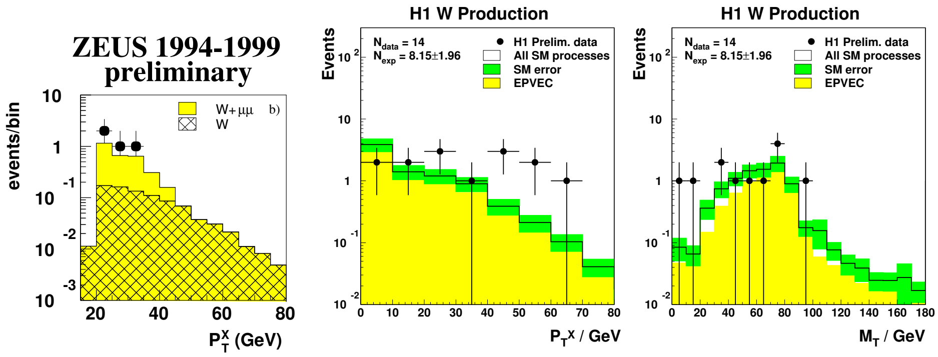

Fig. 13: *Distributions of P_T^X of the ZEUS μ–events and the P_T^X and M_T distributions for H1 of both lepton channels, compared with SM expectations.*

$P_T^X > 25$ GeV	Electrons (Data/MC)	Muons (Data/MC)
ZEUS 94-99	1 / 0.78	0 / 0.82
H1 94-00	$3 / 0.84 \pm 0.22$	$6 / 0.94 \pm 0.26$

Table 1 *: The H1 and ZEUS W analyzes using comparable selection cuts.*

4.2 Single top production

The isolated lepton and the missing transverse momentum of the events described above can be associated either with a W–boson decaying leptonically or background from other SM reactions. The excess of events at large transverse momentum of the hadronic system can tentatively be interpreted as the result of a further mechanism beyond the SM W production. In the SM, the cross section for single top production at HERA is extremely low, but there are extensions of the SM that predict anomalous flavor changing neutral current (FCNC) couplings [31] leading to a measurable single top production cross section at HERA. These FCNC interactions couple a top quark to a light quark (u or c) and a gauge boson and would lead to single top production as shown in Fig. 12. Since the top quark decays dominantly via $t \to bW$, a possible origin of the high P_T^X events described above could be single top production.

To search for single top production events, H1 and ZEUS apply the W selection requirements for leptonic W decay (see Chap. 4.1) with additional cuts of $P_T^X >$ 25(40) GeV for H1 (ZEUS) [30]. Some further cuts are applied by H1 to reject SM W production. H1 searched also in the hadronic W decay channel, requiring 3 hadronic jets where two are required to have a total invariant mass close to the W mass.

No evidence for single top production was found in the hadronic channel. Here H1 measured 10 events with (8.3 ± 4.6) expected from the SM using about half the luminosity used for the lepton channel ($1994-1997$ data only). In the leptonic channel H1 observes 5 events to be compared to the SM expectation of (1.44 ± 0.48). In contrast, ZEUS measures no event, whereas 0.65 are expected. These results are used to calculate

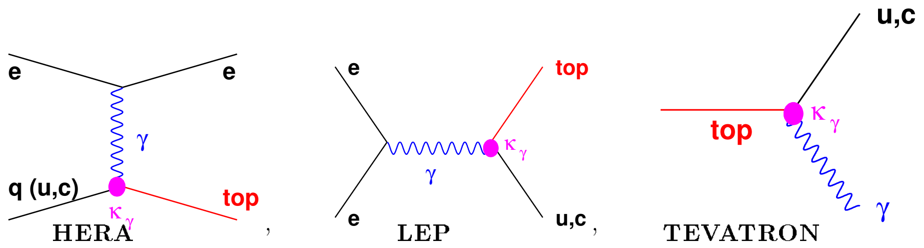

Fig. 14: *Feymann graphs of single top production at HERA (see text) and for the searches at LEP and TEVATROM.*

limits on the magnetic anomalous $tu\gamma$ coupling $\kappa_{\gamma,u}$. Such anomalous couplings can also be measured in e^+e^- and $p\bar{p}$ colliders (see Fig. 14). The HERA results are competitive with those from TEVATRON [32] and LEP[33] as can be seen in Fig. 15. For κ_γ, the HERA limits are more stringent than the limits from LEP and TEVATRON. Whereas LEP and TEVATRON can place limits on both the γ and Z couplings, HERA is sensitive to the γ coupling only due to the suppressed Z propagator.

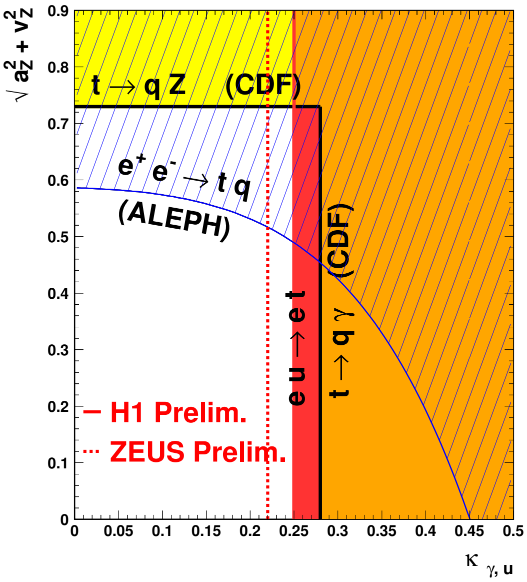

Fig. 15: *Limits on the anomalous magnetic $tu\gamma$ coupling $\kappa_{\gamma,u}$ and on the anomalous vector tuZ coupling $\sqrt{a_Z^2+v_Z^2}$ obtained at the TEVATRON (CDF), LEP (ALEPH) and HERA (H1, ZEUS).*

5 Outlook and summary

5.1 The HERA Upgrade

HERA is upgraded to increase the luminosity by about a factor of five, up to 150 pb^{-1} per year, so that a final total integrated luminosity of about 1 fb^{-1} can be collected for both experiments H1 and ZEUS with polarized electron beams. The expected luminosity opens a wide field of new analyses and high precision measurements:

- **electroweak interactions, proton structure**:
  - NC: study the connection between the helicity structure of the SM and parity violation in NC
  - CC: test for a right–handed contribution to charged current processes: $\sigma_{CC}^{pol.} = (1+P) \cdot \sigma_{CC}$
  - complete the study of proton structure at high Q^2
  - determine the vector and axial NC–couplings for light quarks
- **test of the Standard Model**:
  - probe short distances with high precision
  - probe chiral structure of interactions

5.2 Summary

The inclusive NC and CC cross section measurements for both lepton charges $e^{\pm}$ have been presented and found to be in good agreement with the SM expectations over a large range of Q^2. The extraction of $x\tilde{F}_3$ at large Q^2 and the sensitivity to the valence quarks at high x were shown. At high Q^2 ($Q^2 \approx M_{W,Z}^2$) the NC and CC cross sections are at comparable strength.

Searches for new physics at very high Q^2 were performed for contact interactions and for large extra dimensions. No sign for new physics was found; the data are compatible with the SM within the errors. No evidence for direct leptoquark production was seen. The data were used to set limits on the coupling constant.

Events with an isolated lepton, high P_T^X and missing transverse momentum in the final state were observed in both experiments H1 and ZEUS, but only H1 sees an excess compared to the SM expectation in the high P_T^X region. Motivated by these events, a search for single top production was performed. The results set limits on the anomalous FCNC $tu\gamma$ coupling.

References

[1] H1 Collab., C. Adloff et al., DESY-00-187, submitted to Eur. Phys. J. C, hep–ex/0012052.

[2] H1 Collab., C. Adloff et al., Eur. Phys. J. C13 (2000) 609.

[3] ZEUS Collab., J. Breitweg et al., Eur. Phys. J. C11 (1999) 427.

[4] H. Spiesberger et al., Proceedings of the Workshop "Physics at HERA", vol. 2, DESY (1992) 151.

[5] Review of Particle Properties, D.E. Groom et al., Eur. Phys. J. c15 (2000) 1.

[6] M. Klein et T. Riemann, Z. Phys. C24 (1984) 151.

[7] H1 Collab., C. Adloff et al., DESY-00-181, submitted to Eur. Phys. J. C, hep–ex/0012053.

[8] ZEUS Collab., J. Breitweg et al., Eur. Phys. J. C12 (2000) 411.

[9] H1 Collab., C. Adloff et al., abstract 975 submitted to ICHEP2000, Osaka, Japan.

[10] ZEUS Collab., J. Breitweg et al., abstract 1049 submitted to ICHEP2000, Osaka, Japan.

[11] ZEUS Collab., J. Breitweg et al., abstract 1050 submitted to ICHEP2000, Osaka, Japan.

[12] P. Haberl, F. Schrempp and H.-U. Martyn, Proc. Workshop "Physics at HERA", eds. W. Buchmüller and G. Ingelman, DESY, Hamburg (1991), vol. 2, p. 1133.

[13] N. Arkani–Hamed, S. Dimopolous and G. Dvali, Phys. Lett. B(1998)263, and Phys. Rev. D(1999)086004.

[14] H1 Collab., C. Adloff et al., Phys. Lett. B479 (2000) 358.

[15] H1 Collab., C. Adloff et al., abstracts 951 and 952, submitted to ICHEP2000, Osaka, Japan.

[16] ZEUS Collab., J. Breitweg et al., Eur. Phys. J. C14 (2000) 213.

[17] G.F. Giudice, R. Rattazzi and J.D. Wells, Nucl. Phys. B544 (1999) 3.

[18] H.–L. Lai et al., Eur. Phys. J. C12 (2000) 375.

[19] ZEUS Collab., J. Breitweg et al., Eur. Phys. J. C16 (2000) 253.

[20] ZEUS Collab., J. Breitweg et al., accepted by Phys. Rev. D., DESY 00-133.

[21] ZEUS Collab., J. Breitweg et al., abstract 552 submitted to EPS1999, Tampere, Finland.

[22] H1 Collab., C. Adloff et al., abstracts 953 and 954, submitted to ICHEP2000, Osaka, Japan.

[23] W. Buchmüller, R. Rückl and D. Wyler, Phys. Lett. B191 (1987) 422, Erratum Phys. Let. B448 (1999) 320.

[24] OPAL Collab., G. Abbiendi et al., Eur. Phys. J. C6 (1999)1 and CERN-EP/99-097;
ALEPH Collab., R. Barate et al., Eur. Phys. J. C12 (2000) 183;
DELPHI collab., P. Abreu et al., Eur. Phys. J. C11 (1999) 383;
L3 Collab., L3 Note 2402 (1999), submitted to EPS–HEP 99.

[25] CDF and D0 Collab. hep–ex/9810015, 9pp.,10/1998

[26] H1 Collab., C. Adloff et al., Eur. Phys. J. C11 (1999) 447.

[27] H1 Collab., C. Adloff et al., abstract 974 submitted to ICHEP2000 Osaka, Japan.

[28] ZEUS Collab., J. Breitweg et al., abstract 1041 submitted to ICHEP2000 Osaka, Japan.

[29] H1 Collab., C. Adloff et al., Eur. Phys. J. C5 (1998) 575.

[30] H1 Collab., C. Adloff et al., abstract 961 submitted to ICHEP2000 Osaka, Japan.

[31] T. Han and J.L. Hewitt, Phys. Rev. D60 (1999) 074015;
H. Fritzsch and D. Hermanspötter, Phys. Let. B457 (1999) 186.

[32] CDF Collab., F. Abe et al., Phys. Rev. Lett. 80 (1998) 2525.

[33] ALEPH Collab., ALEPH 2000–07 CONF 2000–04;
DELPHI Collab., DELPHI 2000–032 CONF 351;
L3 Collab., L3 Note 2506;
OPAL Collab., OPAL Physics Note PN429.